https://doi.org/10.14669/AM/166810

PERFORMANCE INVESTIGATION OF HYBRID PHOTOVOLTAIC THERMAL-HEAT WITH MINI-CHANNELS FOR APPLICATION IN ELECTRIC VEHICLES

DARIUSZ STRĄK[1]

Abstract

The first autonomous car was developed in the 1980s, but it wasn't until the early 2010s that the technology began to gain significant attention and investment. In 2010, Google began testing self-driving cars on public roads, and since then, many other companies have joined the race to develop fully autonomous vehicles. Hybrid PVT (Photovoltaic Thermal) heat exchangers cooled with mini-channels find application in autonomous vehicles as a solution that enables efficient cooling of the vehicle's electronics and batteries. The solution involves using photovoltaic panels to generate electricity and removing the heat produced during the process using mini-channels is removed by mini-channels. Hybrid PVT heat exchangers cooled with mini-channels can help maintain appropriate temperatures inside autonomous vehicles that generate large amounts of heat from electronic systems and sensors. The setup can improve the performance and reliability of autonomous systems, increase energy efficiency, and reduce energy demands. The experimental setup includes two parallel mini-channel systems separated by a smooth copper plate. The study aims to determine local heat-transfer coefficients, with a cooled solar cell efficiency range of 10% to 14% compared to other research. The cooled PV temperature range achieved was from 19.6 to 22.4 degrees Celsius, which is favorable for photovoltaic panels' operation under approximate light intensity for Poland's latitude. Heat-transfer from hot surfaces to cold fluids is analyzed during single-phase convection using two calculation methods: one-dimensional and numerical simulations using Simcenter STAR CCM+. Cooling photovoltaic modules is critical for the photovoltaic and autonomous vehicle systems sector, making this research significant both theoretically and practically. The research and methods presented in the article on mini-channel cooling of photovoltaic systems and autonomous vehicle systems are innovative at a global scale, and are crucial for further development of sustainable energy systems and reduction of greenhouse gas emissions.

Keywords: mini-channels; numerical simulations; one-dimensional model; autonomous car system with PVT; vehicle battery heat exchanger

[1] Faculty of Mechatronics and Mechanical Engineering, Kielce University of Technology, al. Tysiąclecia Państwa Polskiego 7, 25-314 Kielce, Poland, e-mail: dstrak@tu.kielce.pl, ORCID: 0000-0001-9762-4693.

https://doi.org/10.14669/AM/166810

1. Introduction

Hybrid PVT collectors are advanced technologies that allow the simultaneous electricity and heat generation from solar radiation. In autonomous vehicles, where electrical energy is crucial, the use of such a hybrid system can provide greater efficiency and energy independence. This can increase the driving range of electric vehicles and reduce their negative impact on the environment. These benefits make hybrid PVT (photovoltaic thermal) collectors currently intensively researched and developed as one of the potential solutions for autonomous vehicles. The cooling of photovoltaic (PV) systems and the development of autonomous vehicles have become increasingly important areas of research due to their potential to significantly contribute to reducing greenhouse gas emissions and promoting sustainable energy systems. The efficient operation of PV systems is heavily dependent on their operating temperature, and effective cooling mechanisms can significantly improve their performance and longevity. Similarly, autonomous vehicles require reliable and efficient power sources to operate their complex systems and reduce their reliance on fossil fuels. The presented scientific article [35] focuses on the analysis of the efficiency of photovoltaic–thermal (PVT) modules, which have the ability to produce both electricity and heat. The research was conducted to determine the influence of temperature, solar radiation intensity, and airflow on the efficiency of PVT modules. In addition, a comparison of the performance of PVT and photovoltaic (PV) modules under the same conditions was carried out. The results of the study showed that PVT modules are more efficient than PV modules in the case of high temperature and low solar radiation intensity. The introduction of airflow leads to a decrease in the module's temperature and an increase in the efficiency of electricity and heat generation. Based on the presented results, it can be concluded that PVT modules have greater production potential than PV modules and can be used in various applications, such as electricity and heat production in buildings or rural areas. The article [26] focuses on the use of a hybrid photovoltaic/thermal collector system in urban technology to harvest sustainable energy. The authors examine various factors that affect the collector's efficiency, such as solar radiation intensity, wind speed, and temperature. They also discuss the benefits of using PV/T in terms of reducing greenhouse gas emissions and economic advantages. The results suggest that the PV/T hybrid collector is an effective way to produce sustainable energy in urban areas. The article [22] describes a solar-powered air cooling system for vehicles. The authors analyze several issues related to the use of the system, including the impact of solar radiation intensity and temperature on the system's cooling efficiency. They also present various configurations of the air cooling system, including systems integrated with photovoltaic collectors to increase efficiency. The conclusions from the research indicate that the solar-powered air cooling system is an effective solution for vehicles and can contribute to reducing fuel consumption and greenhouse gas emissions. The authors of the article [20] describe a study aimed at examining the impact of using photovoltaic cells in city buses on reducing fuel consumption. The results of the study showed that buses equipped with photovoltaic cells consumed less fuel than the control group of buses without them. The authors emphasize the potential benefits of using photovoltaic cells in buses, such as reduced fuel consumption, emission reduction, and cost savings. However, they also point out some challenges associated with implementing this technology, such as the cost of the cells and the

https://doi.org/10.14669/AM/166810

need for training for drivers and maintenance personnel. The authors in publication [10] discusses the modeling and analysis of heat dissipation for liquid cooling lithium-ion batteries. The authors explore the challenges associated with thermal management of these batteries, which can lead to reduced performance, safety concerns, and reduced battery life. They present a detailed model for heat-transfer and fluid flow in a liquid-cooled battery module, and use it to analyze the effects of different design and operating parameters on battery temperature and heat dissipation. The presented research results suggest that liquid cooling can effectively improve the thermal management of lithium-ion batteries and reduce the risk of thermal runaway. The authors in publication [36] discusses the integration of solar energy in electric, hybrid, and autonomous vehicles. The authors review various technological solutions for incorporating solar panels into vehicles, including integration into the car body, roof, and windows. They also analyze the potential benefits of solar energy in vehicles, such as reduced emissions and increased driving range. The article concludes with a discussion on the challenges and limitations of solar integration, such as cost, efficiency, and design constraints. Overall, the authors argue that the integration of solar energy in vehicles is a promising avenue for reducing the environmental impact of transportation. The authors of [34] describes the optimization of the battery thermal management system in electric vehicles. The authors discuss the design process, including numerical modeling, simulations, and prototype testing. The goal of the study was to achieve optimal energy efficiency and battery durability by maintaining an appropriate operating temperature. The research results suggest that optimizing the battery thermal management system can significantly impact the performance of an electric vehicle. The authors in publication [18] presents a three-dimensional thermal modeling of a Li-ion battery cell and a 50 V Li-ion battery pack cooled by a mini-channel cold plate. The study aimed to optimize the cooling system design to improve battery performance and prevent thermal runaway. The results of the simulation showed that the mini-channel cold plate cooling system effectively managed the temperature of the battery pack, reducing the maximum temperature by 20% and improving the battery's lifespan. Overall, the study highlights the importance of proper thermal management for Li-ion batteries in electric vehicles. The article presents a comprehensive review of photovoltaic/thermal (PV/T) hybrid solar collectors. The authors in publication [15] discuss the classification of PV/T collectors based on their design, working principles, and applications. They also review the recent advancements in PV/T technology, such as the development of new systems, materials, and configurations. The article highlights the potential benefits of PV/T collectors, including their high energy efficiency, low environmental impact, and versatile applications in various sectors. Finally, the authors conclude that PV/T collectors have a promising future as a sustainable and cost-effective energy source, and further research and development in this field is necessary to improve their performance and applicability. The authors demonstrated that the microchannel with geometry produced in the plane surface jet in comparison to the straight one may dissipate more heat. It was presented that the flux position influences the total performance of the heat exchanger and needs to be optimized for a specific condition and geometry. The authors in [3] developed a detailed physical model of the PVT/w flat collector by which the overall efficiency was estimated. In publications [11, 12] conducted mathematical and experimental studies of PVT systems. Authors in [30, 31] studied the external conditions that affect the operation of photovoltaic panels. By cooling the solar cells with a stream of fluid, such as air or water, the electricity

https://doi.org/10.14669/AM/166810

yield can be improved. However, a conceptually better design is to reuse the heat energy that the coolant emits [6, 7] investigated the operation of several PVT collector designs. The single-glazed structure has been shown to be superior to the structure without glazing (which has an unfavorable thermal efficiency) or double glazing (which has an unfavorable electrical efficiency). By transient analysis, in publication [25] pointed out that the air collector design has a lower thermal efficiency than the water collector due to the inferior heat-transfer between the thermal absorber and the air stream. The authors of [29] compared the performance of a thermoelectric collector (producing heat first, then electricity) and a PVT/w collector (in a sheet-and-tube design). The electric power of the PVT/w collector was found to be significantly higher than that of the thermoelectric collector. Generally, the reported thermal efficiency of practical PVT/liquid systems is generally in the range of 45–70% for unglazed and glazed collector designs. For flat PVT/air systems, the optimum thermal efficiency can reach 55%. Authors investigated the design of a new panel cooling based on a heat pipe in article [1]. The thermosiphon or gravity-assisted heat pipe is a completely passive system that transfers heat from one place to another. The proposed cooling system for the rear part of the solar cells included two interconnected heat exchangers, preempted and filled with R-11, R-22, and water refrigerants. The authors in publication [2] presented a simulation study of the use of PVT/in collectors as water heating devices in a solar-assisted heat pump system. In the publication [16] evaluated the improvement of the energy efficiency of a system in which solar cells were attached to a metal trapezoidal sheet on the vertical facades of buildings. In [17] presented Eulerian two-fluid model coupled with the extended wall boiling model was used to simulate the departure from nucleate boiling (DNB) in vertical heated tubes under high pressure using Simcenter STAR-CCM+. CFD calculations were performed with different wall heat fluxes. A two-fluid model coupled with an extended wall boiling model was used to simulate DNB in vertical heated tubes with both uniform and nonuniform heat fluxes. The authors of [13] presented research on the use of a hybrid phase change material and nanofluid for cooling photovoltaic modules to control temperature and improve their efficiency. The results show that this technology allows for achieving a more uniform temperature and reducing the risk of damage caused by overheating. The properties of hybrid phase change materials and nanofluids, cooling efficiency, costs and scalability of this technology are also discussed in the article. The authors in publication [33] presents research on boiling of distilled water in asymmetrically heated rectangular mini-channels. The experiments showed that asymmetric heating affects heat transfer intensity, and the liquid temperature depends on the flow rate. The authors also analyzed the impact of other factors on heat transfer during boiling. These studies are relevant to the design of device cooling systems where fluid flow efficiency is critical for maintaining optimal temperature. The article [23] describes a study conducted on a heat exchanger with two rectangular mini-channels, in which a low-boiling FC-72 fluid flows in the hot mini-channel parallel to water in the cold mini-channel. The authors use two calculation methods, one-dimensional (1D) and two-dimensional (2D), to investigate the heat-transfer characteristics in the system, the influence of channel size, flow velocity, and inlet temperature on the heat-transfer performance in two parallel mini-channels. The results show that the thermal performance of the heat exchanger depends largely on the channel dimensions and flow conditions. The authors suggest that optimizing the mini-channel design and flow conditions could improve the heat-transfer performance in parallel flow heat exchangers. The article [37] describes

https://doi.org/10.14669/AM/166810

a PVT collector that utilizes aluminum mini-channels and nonimaging optics. PVT allows for simultaneous production of electricity and heat and is becoming increasingly popular in the field of renewable energy. However, traditional PVT collectors are costly. The authors propose the use of aluminum mini-channels and nonimaging optics to create an ultra-low-cost PVT collector. The research showed that such a collector was effective in producing both electricity and heat, which can contribute to increasing the utilization of renewable energy sources and reducing costs in this field. In the presented publication [5], the performance of a solar system depends mainly on the climate, particularly on the availability of solar radiation. The average annual solar irradiation on the horizontal plane in Poland ranges from 950 kWh/m^2 to 1150 kWh/m^2. During the summer months in Warsaw, the average monthly global solar irradiation ranges from 140 kWh/m^2 to 180 kWh/m^2, with the solar irradiance at noon reaching levels as high as 700 W/m^2 to 950 W/m^2. Conversely, the lowest monthly solar irradiation occurs in December, with only 11–12 kWh/m^2 for Warsaw. At this time, the solar irradiance is markedly low, with a maximum of 200 W/m^2 at noon. At this time, the solar irradiance is markedly low, with a maximum of 200 W/m^2 at noon. The article [24] describes research on heat-transfer characteristics in miniaturized channels during boiling of a refrigerant in different flow orientations. The authors conducted experiments using rectangular mini-channels of various sizes and the refrigerant R-134a, while changing the flow orientation of the liquid. The aim of the research was to determine the influence of flow direction on heat-transfer characteristics, such as heat-transfer coefficient and Nusselt number. The results of the research showed that flow orientation has a significant impact on heat-transfer characteristics in miniaturized channels. It was found that the heat-transfer coefficient is higher in longitudinal flow than in transverse flow. Additionally, it was observed that for smaller mini-channel sizes, the values of the heat-transfer coefficient were higher. The article [8] describes a study on the impact of configurations on the performance of microchannel counter-flow heat exchangers. The results showed that configuration has a significant impact on the performance of microchannel counter-flow heat exchangers. It was found that a greater number of channels and more complex channel configurations increase flow resistance, which lowers heat exchanger efficiency. On the other hand, a higher number of channels can increase heat-transfer efficiency, as it increases the heat exchange surface area. In addition, PVT hybrid heat exchangers can be used in autonomous cars as an additional power source for autonomous systems such as cameras, sensors and control systems, which allows to extend the driving time and increase the reliability of such vehicles and cool car batteries, car control systems, processors, electronic components, car engine and all internal devices. On the other hand, a higher number of channels can increase heat-transfer efficiency, as it increases the heat exchange surface area.

In addition, PVT hybrid heat exchangers can be used in autonomous cars as an additional power source for autonomous systems such as cameras, sensors and control systems, which allow extending the driving time and increase the reliability of such vehicles and cool car batteries, car control systems, processors, electronic components, car engine and all internal devices. Therefore, the research and methods presented in the article on mini-channel cooling of photovoltaic systems and autonomous vehicle systems are innovative at a global scale, and are crucial for further development of sustainable energy systems and reduction of greenhouse gas emissions.

https://doi.org/10.14669/AM/166810

2. Experimental stand and test section

With the use of a PVT heat exchanger with mini-channels, it is possible to cool the car batteries, car control systems, processors, electronic components, car engines, and all internal devices. The article presents a system that maintains the battery temperature at an optimal level using two cooling circuits. These types of hybrid PVT systems are used in autonomous cars and allow for a decrease in component temperatures during the summer, preventing overheating, and can warm up batteries in the winter, preventing freezing and reducing energy consumption at the same time. The test experimental stand used for the experiments includes two fluid flow circuits (hot and cold), a data acquisition and handling system, a power supply and control system, and a lighting system. The purpose of the measurements is to analyze the performance of two parallel mini-channel systems separated by a cooper plate with

a smooth surface. The temperature of the smooth surface of the solar panel is monitored using thermal imaging. The main components of the module being tested are a heated plate (cover glass) with PV cells, a system of hot mini-channels, a copper separating plate, a system of cold mini-channels, a copper closing bottom plate, as well as K-type thermocouples and pressure sensors fitted at the inlets and outlets of the mini-channels. The tests involve gradually increasing the temperature of the top surface of the photovoltaic panel exposed to a heat flux generated by an artificial halogen light source. The experimental results will be used to determine the local heat-transfer coefficients and the overall heat- transfer coefficient for the photovoltaic-thermal system. The research will also analyze the effects of selected process parameters and the thermal properties of the refrigerants on single-phase convective heat-transfer for the heated PV panel. The proposed calculation methods will be used to determine the local heat-transfer coefficients at the interfaces between the heated surface and the hot mini-channels, between the hot mini-channels and the separating plate, and between the separating plate and the cold mini-channels. The main parameters and errors of the experiments are presented in publication [23].

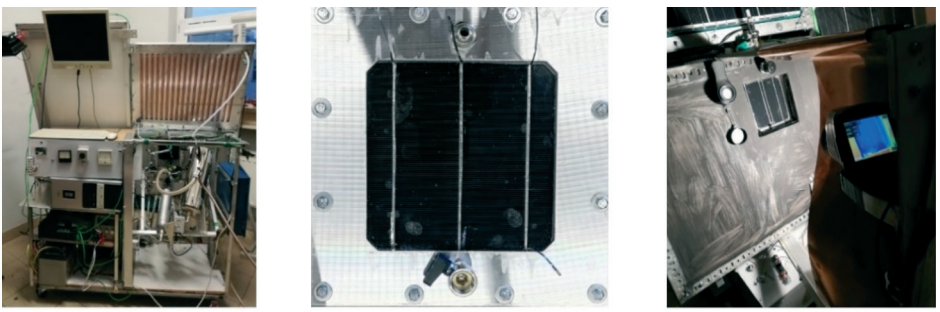

a) b) c)

Fig. 1. A view of the main systems of the experimental setup: (a) rear view of the experimental setup, (b) a view of the test section with a PVT with mini-channels, (c) a view of the front of the test module with a thermal shield and a thermal camera

https://doi.org/10.14669/AM/166810

Figures 1a and 1c present a view of the test module from the PV panel. The PV panel with glass has dimensions of 0.156 m in width and 0.156 mm in length, as well as a silicon solar cell thickness of δ_{Si} = 0.00012 m and a tempered glass thickness of δ_{glass} = 0.0032 m for a total of about δ = 0.0034 m in thickness. The individual components of the test module are presented in the publication [34]. Its main elements are two parallel copper plates and the PV cell plate. A group of 12 parallel mini-channels in Figure 2b six "hot" mini-channels and six "cold" ones with a rectangular cross section, each 1.5 mm deep, 20 mm width and 70 mm length is produced between them.

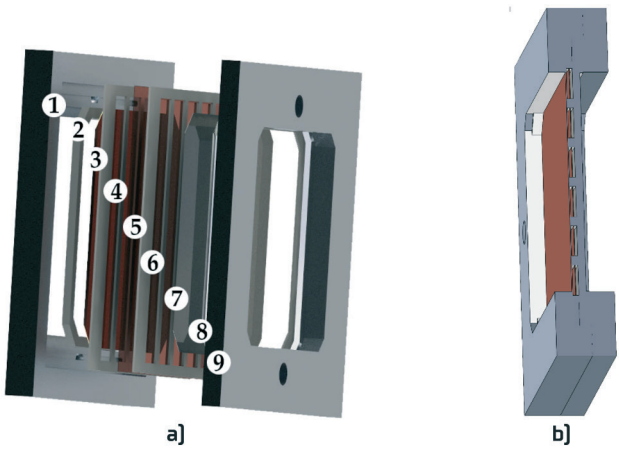

Fig. 2. View of the compact heat exchanger: (a) components 1,9 – aluminum covers, 2,8 – silicone gaskets, 3 – PV solar cell with glass, 4 – silicone gasket forming the hot mini-channel, 5 – copper plate between two mini-channels, 6 – silicone gasket forming the cold mini-channel, 7 – copper plate, (b) group of mini-channels

The individual components of the test module presented publication [34] and Figure 2. Its main elements are two parallel copper plates and the PV cell plate. A group of 12 parallel mini-channels six "hot" mini-channels and six "cold" ones with a rectangular cross section, each 1.5 mm deep, 20 mm width and 70 mm length is produced between them.

https://doi.org/10.14669/AM/166810

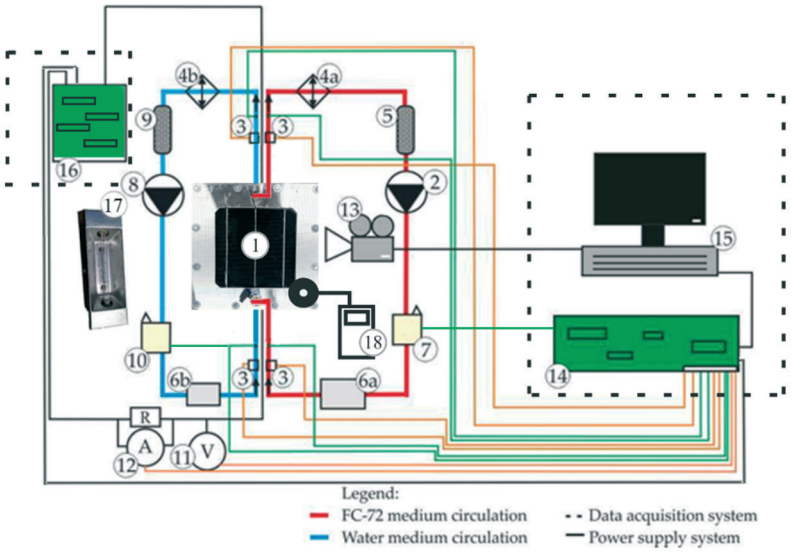

a)

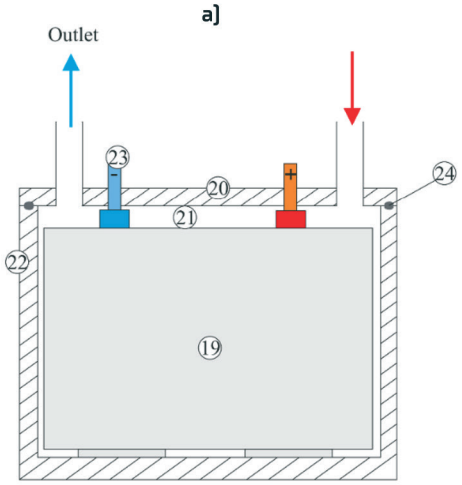

b)

Fig. 3. Schematic diagram of the: (a) experimental stand: 1 – test section with mini-channels; 2,8 – circulating pumps; 3 – pressure meter; 4a, 4b – battery heat exchanger; 5,9 – filters; 6a – mass flow meter; 6b – magnetic mass flow meter; 7,10 – battery thermal management system; 11 – ammeter; 12 – voltmeter; 13 – infrared camera; 14 – data acquisition station; 15 – PC computer; 16 – data acquisition station 2; 17 – heating bulb; 18 – luxmeter; (R) – a shunt. (b) battery heat exchanger: 19 – battery; 20 – upper cover of the heat exchanger; 21 – Fluorinert FC-72; 22- heat exchanger housing; 23 – electrode; 24 – silicone gasket

https://doi.org/10.14669/AM/166810

Figure 3a presents the experimental setup utilized in the study. The test section comprises two mini-channels (1) and is equipped with circulating pumps (2, 8), pressure meters (3), heat exchangers

(4a, 4b), filters (5, 9), a mass flow meter (6a), a magnetic mass flow meter (6b), and battery thermal management system (7, 10). Additionally, the setup includes an ammeter (11), a voltmeter (12), and an infrared camera (13). Of particular significance are two closed loops of working fluids: the hot fluid circuit, in which the working fluid FC-72 circulates (low current resistivity), and the cold fluid circuit, in which distilled water flows. In addition to the aforementioned equipment, the experimental setup is complemented by a data acquisition station *DaqLab/2005 IOtech* (14), a PC computer (15), The data acquisition station *IOTech Daqboard/3000* (16) is connected to a solar panel and measures voltage and current and the heating bulb (17) heats the surface of the solar panel. After dearation of the flow circuit installation and the test section, as well as stabilizing the pressure and flow rate of the fluids, the heat flux supplied to the heated plate is gradually increased by fluid adjustment of the current. The conter-current flow of working fluids in mini-channels is forced by the operation of pumps. A thermal imaging camera is used to monitor the temperature of the outer heated plate PV cells surface. The heating bulb was set up during the experimental tests at a distance of approximately 0.4 m from the surface of the solar panel. The power of the heating bulb was 500 W. The photovoltaic panel with tempered glass has dimensions of 0.156 m in width, 0.156 m in length, and 0.004 m in thickness. A counter-current flow of working fluids is applied in the mini-channels, with laminar flow in both fluids. Figure 3b presents a prototype battery heat exchanger.

3. The methods of heat-transfer coefficient determination

3.1. Simcenter STAR CCM+ numerical calculations

The methodology of the STAR-CCM+ program involves numerically solving the governing equations of fluid flow using the finite-volume method. This entails transforming all governing equations into

a system of nonlinear algebraic equations that approximate various behaviors of the given system [9, 4]. To generate the design, a 3D-CAD model (imported from Solidworks software) based on the functions within the STAR-CCM+ program was used. Operations were then performed on the created geometry to cut out the hot and cold domains (Figure 4b). The characteristics of the test module plates and experimental data presented in Table 1. Multiple iterations of numerical calculations for the same model, with the input mass flow values, enable obtaining the pressure characteristics as a function of flow. Figure 4a presents the residual dependence as a function of iteration. Up to 9334 iterations have been achieved.

https://doi.org/10.14669/AM/166810

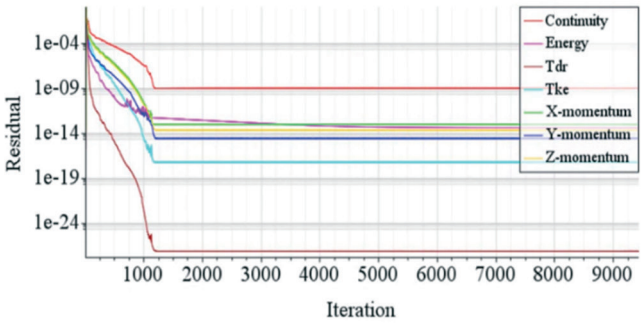

a)

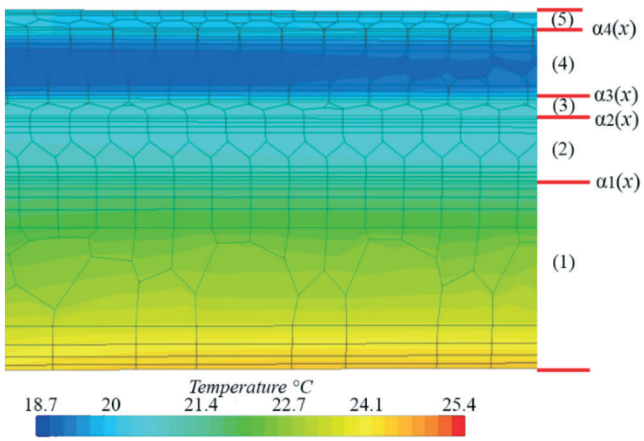

b)

Fig. 4. View of: (a) the residuals as a function of iteration, (b) two-dimensional view of the channel body and the working fluids in the test section (solid and fluid regions) showing polyhedral mesh, temperature distribution on marked elements: (1) – glass with photovoltaic cell; (2) – mini-channel "hot" with Fluorinert FC-72; (3) center cooper Cu plate; (4) – mini-channel "cold" with distilled water; (5) – closing cooper Cu plate; $\alpha_1(x)$ at the photovoltaic cell – FC-72 contact surface; $\alpha_2(x)$ at the FC-72 – copper plate contact surface; $\alpha_3(x)$ at the copper plate – water contact surface; $\alpha_4(x)$ at the water – closing plate

In Table 1, the most important parameters of three plates used in the test module are presented. Each of the copper plates separates mini-channels, while the heated plate PV and the closing plate Cu close the mini-channels from the outer side.

https://doi.org/10.14669/AM/166810

Table 1. The characteristics of the test module plates and experimental data.

Properties/ Experimental data	Heated plate PV	Copper plate	Closing plate Cu
Thickness, main physical properties			
Thickness, σ m	0.004	0.0003	0.0005
Density kg/m³	2500	8940	8940
Thermal conductivity, λW/[m²K]	1.45	382	382

The main fluid properties and experimental data parameters, as well as the numerical Simcenter Star CCM+ experimental data, are presented in Table 2.

Table 2. Main fluid properties and experimental data.

Properties/ Experimental data	Fluid FC-72	Distilled water
Density, ρ kg/m³	1732.5–1737.8	998.5 – 998.6
Thermal conductivity, λW/[m²K]	0.061	0.6
Boiling Temperature, °C	56	98.6–100.0

The initial conditions applied in the STAR CCM+ program were very similar to the actual operating environment during testing on the module at the experimental stand in Table 3. These conditions allowed the initiation and stabilization of the computational system, thereby enabling a comparison between the calculated simulation data and the measured data from the experimental stand which are presented in Table 3.

Table 3. Initial Conditions main experimental data

Region name	Initial conditions	Value
Exchanger aluminum housing		
	Static Temperature	20.0°C–25.8°C
	Solid (Al)	Density: 2702 kg/m³, specific heat: 903.0 J/kgK, thermal conductivity: 237 W/mK
Mini-channel "hot" FC-72		
Inlet	Mass Flow Rate, m_{FC}	0.0032 kg/s
	Total Temperature, T_{in}	18.7°C
	Turbulence Intensity	0.01
	Turbulent Viscosity Ratio	1.0
Outlet	Pressure, P_{out}	0.09 bar
	Static temperature, T_{out}	23.1°C
	Turbulence Intensity	0.01
	Turbulent Viscosity Ratio	1.0

https://doi.org/10.14669/AM/166810

Table 3. Initial Conditions main experimental data; cont.

Region name	Initial conditions	Value
	Mini-channel "cold" water	
Inlet	Mass Flow Rate, m_w	0.0087 kg/s
	Total Temperature, T_{in}	18°C
	Turbulence Intensity	0.01
	Turbulent Viscosity Ratio	1.0
Outlet	Pressure, P_{out}	0.05 bar
	Static temperature, T_{out}	19.62°C
	Turbulence Intensity	0.01
	Turbulent Viscosity Ratio	1.0
	Photovoltaic Panel (PV)	
	Heat Flux, q	1000 W/m^2
	Solid (Si)	Density: 8900 kg/m^3, specific heat: 443 J/kgK, thermal conductivity: 1.45W/mK

3.2. One-dimensional model

In the proposed one-dimensional model, heat-transfer in one direction was considered perpendicular to the direction of fluid flow and the width of the mini-channel. It was assumed that the insulation process of the test section allows the simplification for the entire heat generated in the heating plate to be transferred to the flowing fluid in the "hot" mini-channel. The formula (1) below is used to calculate the heat flux for the heating plate. The radiation intensity (Luxmeter – to measure light intensity, *Delta OHM HD 2102.1* measures Lux and the second device, *Voltcraft (PL-110SM)*, measures illuminance in W/m^2), E of the receiver is equal to the radiant flux per unit area, which is the surface density of the radiant flux q, as reported in the publication [14, 27, 28] equation (1):

$$E = q \tag{1}$$

Knowledge of the temperature distribution of the external surface of plate $T_{H,IR}(x)$ allows determination of the heat-transfer coefficient at the interface of the heating plate fluid in a hot mini-channel using equation (2) for the surface of a solar cell (Figure 3) [23, 32].

$$\alpha_{1,1D}(x) = \frac{q\lambda_H}{\lambda_H\left(T_{H,IR}(x) - T_{FC,lin}(x)\right) - q\delta_H} \tag{2}$$

where the hot fluid (FC-72) temperature $T_{FC,lin}(x)$ is calculated from (3):

$$T_{FC,lin}(x) = \frac{T_{FC,out} - T_{FC,in}}{L} \cdot x + T_{FC,in} \tag{3}$$

The next step in the calculations involves determining the heat-transfer coefficient $\alpha_{2,1D}(x)$ at the interface between the FC-72 and the copper plate and the center partition using the formula (4) [23, 32]:

$$\alpha_{2,1D}(x) = \frac{Q_{FC}}{A_2\left(T_{FC,lin(x)} - T_{Cu,lin(x)}\right)} \tag{4}$$

https://doi.org/10.14669/AM/166810

Temperature of the center partition $T_{Cu,lin}(x)$ is approximated linearly based on the known temperature measured using two type K thermocouples [32] placed at the ends of the center plate and soldered to the hot fluid side, $T_{TC,1}$ and $T_{TC,2}$, according to the following equation in publication [23, 32]:

The next step in the calculations involves determining the heat-transfer coefficient $\alpha_{3,1D}(x)$ at the interface between the copper plate (center partition) and to the cold fluid side using the formula (5), [32]:

$$\alpha_{3,1D}(x) = (\frac{1}{k} - \frac{1}{\alpha_{1,1D}(x)} - \frac{1}{\alpha_{2,1D}(x)} - (\delta_{Cu} \cdot \frac{1}{\lambda_{\mathrm{Cu}}}))^{-1} \tag{5}$$

Next, to determine the heat-transfer coefficient $\alpha_{4,1D}(x)$ at the interface of the fluid in the mini-channel with the cold end plate, a calculation method was used based on equation (6). The heat-transfer resistance of the closing plate $\frac{1}{\alpha_{4,1D}(x)}$ can be calculated using the following formula (6) [32]:

$$\frac{1}{k} = \frac{1}{\alpha_{1,1D}(x)} + \frac{1}{\alpha_{2,1D}(x)} + \frac{\delta_{Cu}}{\lambda_{Cu}} + \frac{1}{\alpha_{3,1D}(x)} + \frac{1}{\alpha_{4,1D}(x)} \tag{6}$$

The heat-transfer coefficient in the contact area between the water and the a closing plate has the equation (7):

$$\alpha_{4,1D}(x) = -(\frac{1}{\alpha_{1,1D}(x)} + \frac{1}{\alpha_{2,1D}(x)} + (\delta_{Cu} \cdot \frac{1}{\lambda_{Cu}}) - \frac{1}{k} + \frac{1}{\alpha_{3,1D}(x)})^{-1} \tag{7}$$

The overall heat-transfer coefficient k is calculated for a flat surface and determines the amount of heat passing through a partition with a unit surface area when there is a temperature difference between the surfaces equal to one unit of temperature has been presented in publication [21, 32] see equation (8):

$$k = \frac{Q_{FC}+Q_W}{2A\,\Delta T} \tag{8}$$

where ΔT presented the average logarithmic difference in liquid temperatures (11) calculated as in [19, 32] equation (10a) and (10b) and the heat flux received from the cold fluid Q_{FC}, Q_W is from the publication [32] equation (9a) and (9b):

$$\text{(a) } Q_{FC} = m_{FC}c_{p,FC}(T_{\mathrm{FC},in}\text{-}T_{\mathrm{FC},out}) \quad \text{(b) } Q_w = m_w c_{p,w}(T_{w,in}\text{-}T_{w,out}) \tag{9}$$

where the mass flow rate of "hot" and "cold" fluid is:

$$\text{(a) } m_{FC} = \rho_{FC} \cdot v_{FC} \cdot A_{FC} \qquad \text{(b) } m_w = \rho_w \cdot v_w \cdot A_w \tag{10}$$

$$\Delta T = \frac{\Delta T_W - \Delta T_{FC}}{Ln\frac{\Delta T_W}{\Delta T_{FC}}} \tag{11}$$

where the temperature difference between fluids flowing in opposite directions is: $\Delta T_{FC} = (T_{FC,in} - T_{w,out})$ and, $\Delta T_W = (T_{FC,out} - T_{w,in})$, in publication [38].

https://doi.org/10.14669/AM/166810

4. Results and discussion

The numerical calculations results have been presented in the form of screenshots obtained from the Simcenter STAR-CCM+ software. These screenshots were generated using the longitudinal symmetry axis of the test section as the reference. The 2D temperature distributions on the outer surface of the photovoltaic panel were obtained through experimental measurements using an infrared camera (Figure 5b) and through simulations using Simcenter STAR CCM+ (Figure 5a).

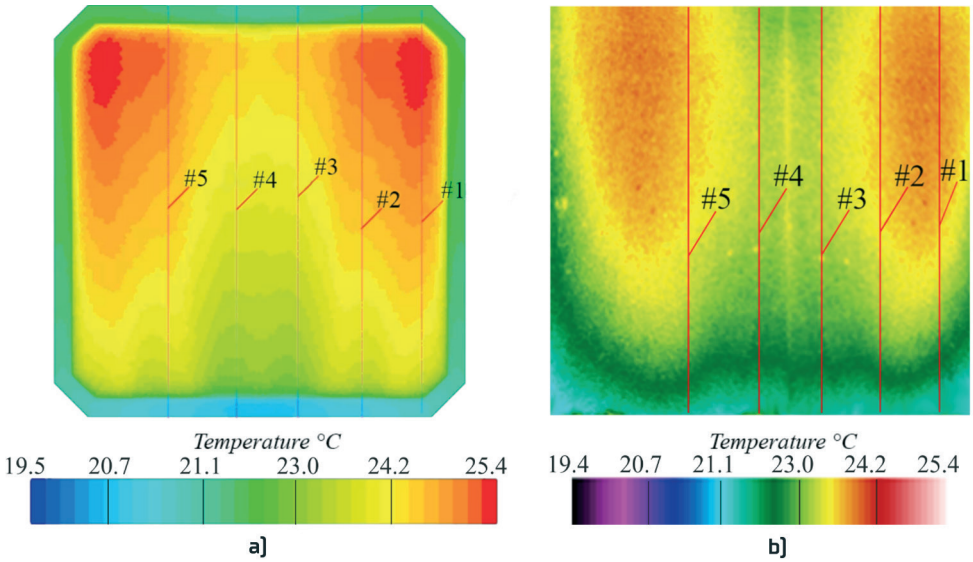

Fig. 5. Three-dimensional temperature distribution on the heater surface obtained: (a) as a result of numerical computations due to Simcenter STAR-CCM+ software, (b) from the experiment with the use of an infrared camera

It can be noticed that the FC-72 fluid entering the cold mini-channel is heated by the photovoltaic cell mainly at the contact surface. The liquid next to the heated wall has an increased temperature, which decreases significantly with increasing distance. In the hot mini-channels axis, the temperature of the fluid increases with distance from the inlet, mainly on the sides of the solar cell. In this study, we compared the temperature field obtained from numerical computations with the experimental data collected from the experiment with the use of an infrared camera *FLIR E60*. Figure 5a displays the 2D temperature distribution in the test section, captured from the outer surface of the heater. The photovoltaic panel surface temperature increases gradually from the inlet to the outlet of the mini-channels. To facilitate comparison, we present the temperature distribution on the photovoltaic panel surface recorded by an infrared camera during the laboratory experiment in Figure 5b.

https://doi.org/10.14669/AM/166810

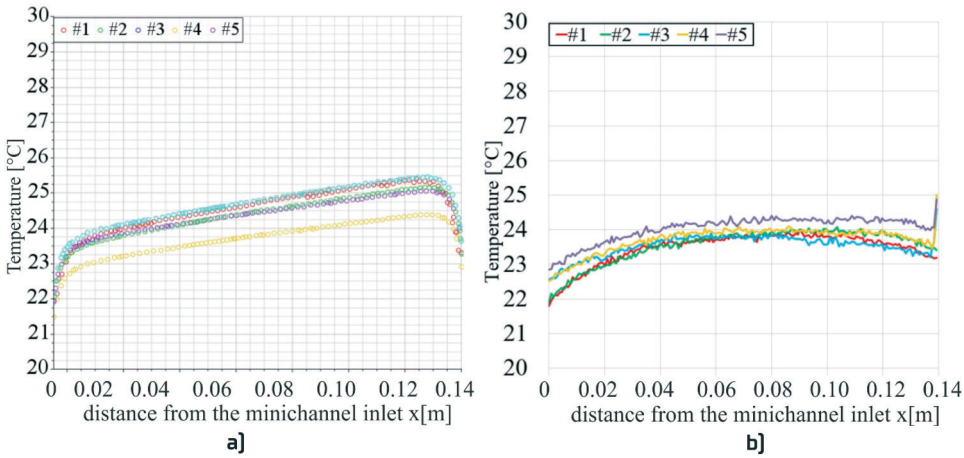

Fig. 6. The heated area photovoltaic cell temperature versus the distance from the mini-channel inlet obtained from: (a) numerical computations (according to Simcenter STAR-CCM+ software), (b) the experimental measurement (using an infrared camera IR)

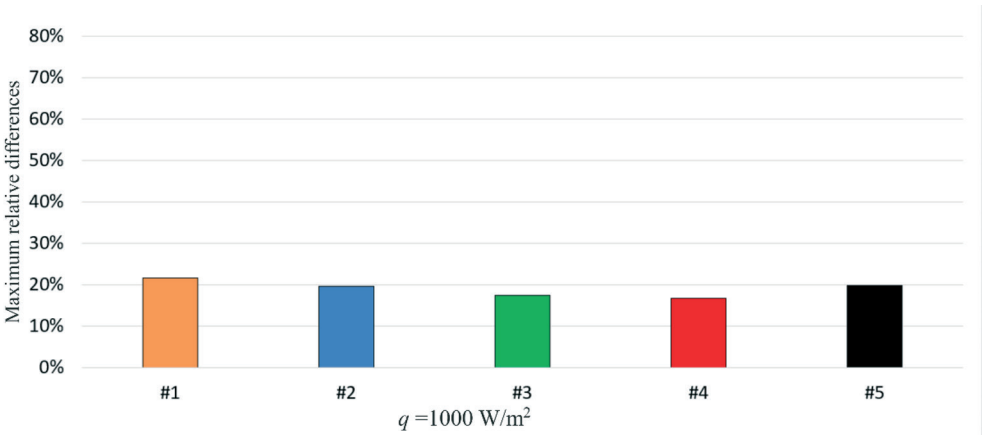

Fig. 7. Maximum relative differences between temperature of the photovoltaic cell surface from the experiment with the use of an infrared camera and from with the numerical simulation Simcenter STAR CCM+

Figure 6, compared two dependencies of the photovoltaic panel temperature both of which were based on the input data from experiment Series No 32. Analyzing the temperature results depicted in Figure 7, we observe that the distribution and the surface temperature values are similar and are about 19%.

https://doi.org/10.14669/AM/166810

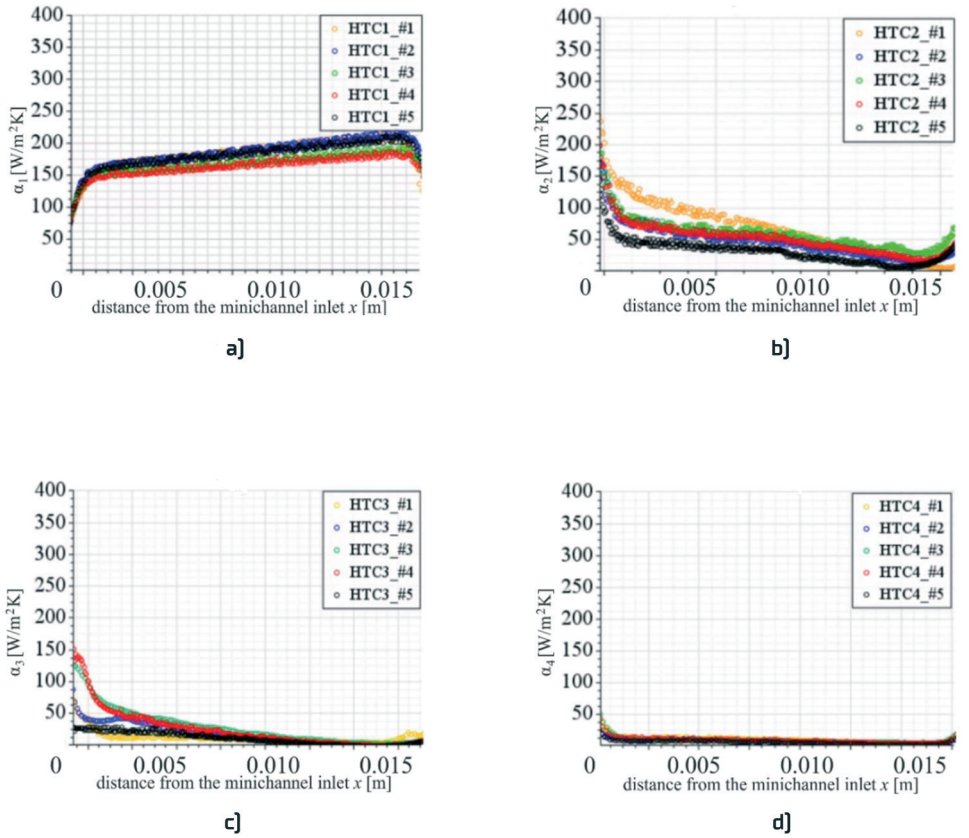

Fig. 8. View of: (a) heat-transfer coefficients $\alpha_{1,\mathrm{STAR}}(x)$ versus the distance from the mini-channel inlet: at the photovoltaic cell – FC-72 contact surface, equation (2), (b) heat-transfer coefficients $\alpha_{2,\mathrm{STAR}}(x)$ at the FC-72 – copper plate contact surface, equation (4), (c) heat-transfer coefficients $\alpha_{3,\mathrm{STAR}}(x)$ at the copper plate – water contact surface, equation (5), (d) heat-transfer coefficients $\alpha_{4,\mathrm{STAR}}(x)$ at the water – closing plate surface, equation (7); calculated according to: numerical simulation Simcenter Star CCM+; heat flux q = 1000 W/m²

https://doi.org/10.14669/AM/166810

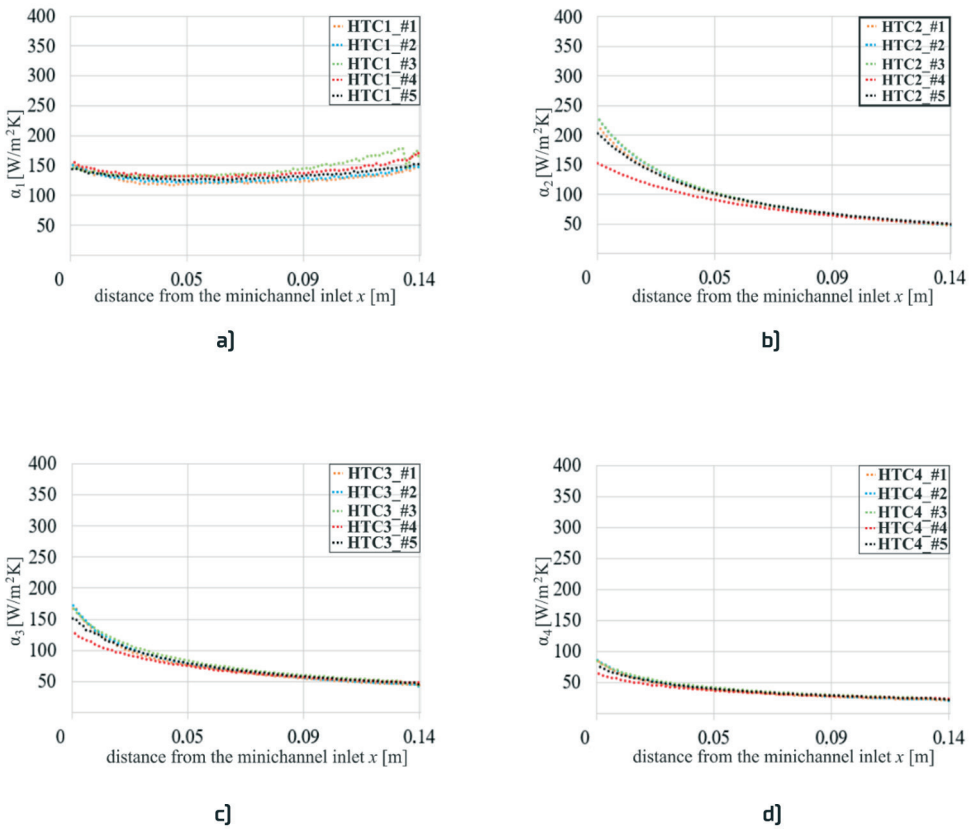

Fig. 9. View of: (a) heat-transfer coefficients $\alpha_{1,1D}(x)$ versus the distance from the mini-channel inlet at the photovoltaic cell – FC-72 contact surface, equation; (2); (b) $\alpha_{2,1D}(x)$ at the FC-72 – copper plate contact surface, equation (4); (c) $\alpha_{3,1D}(x)$ at the copper plate – water contact surface, equation (5); (d) $\alpha_{4,1D}(x)$ at the water – closing plate surface equation (7); calculated according to: 1D approach; heat flux q = 1000 W/m²

Analysis of Figure 9a shows that the heat-transfer coefficient values of $\alpha_1(x)$ increase with the distance from the channel inlet, reaching a maximum value of $\alpha_{1,1D}$ = 163 W/(m²K) for the 1D approach, and $\alpha_{1,STAR}$ = 223 W/(m²K) in Figure 8a for the numerical simulation. The minimum values are $\alpha_{1,1D}$ = 118 W/(m²K) in Figure 9a for the 1D approach and $\alpha_{1,STAR}$ = 106 W/(m²K) in Figure 8a for the numerical simulation. The maximum relative differences between the two approaches do not exceed 48% in Figure 10. For $\alpha_2(x)$, the heat-transfer coefficient values also increase with the distance from the channel inlet, with a maximum value of $\alpha_{2,STAR}$ = 238.3 W/(m²K) in Figure 8b for the numerical simulation and $\alpha_{2,1D}$ = 325.8 W/(m²K) in Figure 9b for the 1D approach. The minimum values are $\alpha_{2,1D}$ = 48.3 W/(m²K) in Figure 9b for the 1D approach and $\alpha_{2,STAR}$ = 28.5 W/(m²K) in Figure 8b for the

https://doi.org/10.14669/AM/166810

numerical simulation. The maximum relative differences between the two approaches do not exceed 77.1% in Figure 10. Similarly, for $\alpha_3(x)$, the heat-transfer coefficient values increase with the distance from the channel inlet, reaching a maximum value of $\alpha_{3,STAR}$ = 244 W/(m²K) in Figure 8c for the numerical simulation and $\alpha_{3,1D}$ = 180 W/(m²K) in Figure 9c for the 1D approach. The minimum values are $\alpha_{3,STAR}$ = 73.4 W/(m²K) in Figure 8c for the numerical simulation and $\alpha_{3,1D}$ = 90 W/(m²K) in Figure 9c for the 1D approach. The maximum relative differences between the two approaches do not exceed 65.3% in Figure 10 and decrease with increasing heat flux. For $\alpha_4(x)$, the heat-transfer coefficient values also increase with the distance from the channel inlet, with a maximum value of $\alpha_{4,STAR}$ = 73.2 W/(m²K) in Figure 8d for the numerical simulation and $\alpha_{4,1D}$ = 90 W/(m²K) in Figure 9d for the 1D approach. The maximum relative differences between the two approaches do not exceed 65.3% in Figure 10.

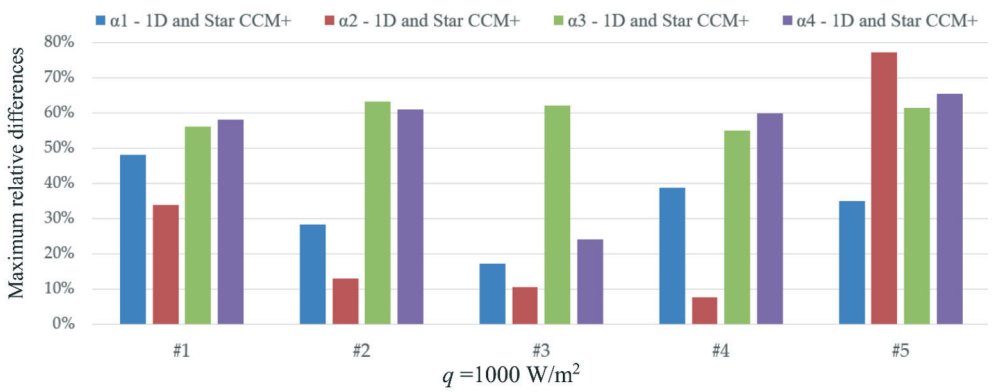

Fig. 10. Maximum relative differences between heat-transfer coefficients one-dimensional method and from with the numerical simulation Simcenter STAR CCM+:
$\alpha_1(x)$ at the photovoltaic cell – FC-72 contact surface;
$\alpha_2(x)$ at the FC-72 – copper plate contact surface;
$\alpha_3(x)$ at the copper plate – water contact surface;
$\alpha_4(x)$ at the water – closing plate surface

When analyzing the results shown in Figure 10 that illustrate the comparative results according to the 1D approach and obtained using with the numerical simulation, the values of the maximum relative differences were lower in the lines #1 and #5b in Figure 5. The highest was reached, up to 77.1%, for heat-transfer coefficients $\alpha_2(x)$ at the FC-72 – copper plate contact surface and α_4 at the water – closing plate surface up to 65.3%. The minimum was reached, down to 7.6%, for heat-transfer coefficients $\alpha_2(x)$ at the photovoltaic cell – FC-72 contact surface. The lowest score percent was obtained in the comparative analysis of the 1D approach and numerical simulation for the #3, #4 photovoltaic center cell surface, where all heat-transfer coefficients are at their minimum.

https://doi.org/10.14669/AM/166810

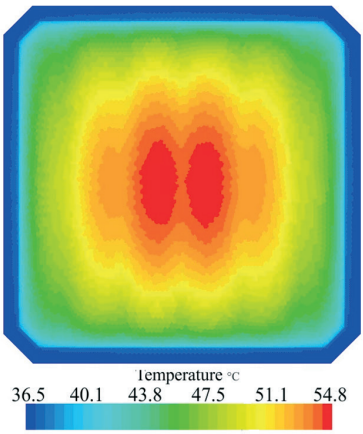

Fig 11. Three-dimensional temperature distribution on the uncooled solar cell surface PV obtained as the result of numerical computations due to Simcenter STAR-CCM+ software

The temperature coefficient of solar cell efficiency is an indicator of how efficiently a solar cell converts solar energy into electrical energy depending on temperature. This coefficient determines how much of the maximum power of a solar cell is lost as temperature increases. For a solar cell with cooling Figure 5, the temperature range is from 19.6°C to 25.4°C. In this case, the temperature coefficient of efficiency is relatively low, at around –0.2%/°C, meaning that as temperature increases by 1°C the power output of the solar cell decreases by 0.2%. For a solar cell without cooling, the temperature range is from 36.5°C to 54.8°C in Figure 11. In this case the temperature coefficient of efficiency is significantly higher, at around –0.5%/°C, meaning that as temperature increases by 1°C, the power output of the solar cell decreases by 0.5%. Comparing these two cases, it can be seen that a solar cell with cooling is much more stable within the temperature range in which it is used mini-channel cooled Figure 5, which translates to higher efficiency and lower power losses. A solar cell without cooling is more sensitive to temperature, and in the case of high temperatures, can suffer much greater power losses. The conclusion is that the use of cooling for solar panels can significantly improve their efficiency and performance, which is particularly important in applications where panels are exposed to high temperatures, such as in autonomous vehicle solar installations in hot climates. The known value of the heat-transfer coefficient at the interface between the PV cell and the fluid, as shown in Figures 8a and 9a, can be used in the equation that describes the efficiency of the solar cell to calculate its effectiveness. The equation (12) is given below:

$$\eta = \frac{(\frac{P}{A}E)}{\frac{1+\alpha_1(x)(T_{IR}-T_a)}{E}} \tag{12}$$

where: η – efficiency of the solar cell, P – power of the solar cell, A – area of the solar cell, E – solar irradiance, T_{IR} – the temperature is linearly extracted from the thermogram of Flir60 thermal imaging camera, T_a – temperature ambient, $\alpha_1(x)$ – heat-transfer coefficient at the interface between the PV cell and the fluid.

https://doi.org/10.14669/AM/166810

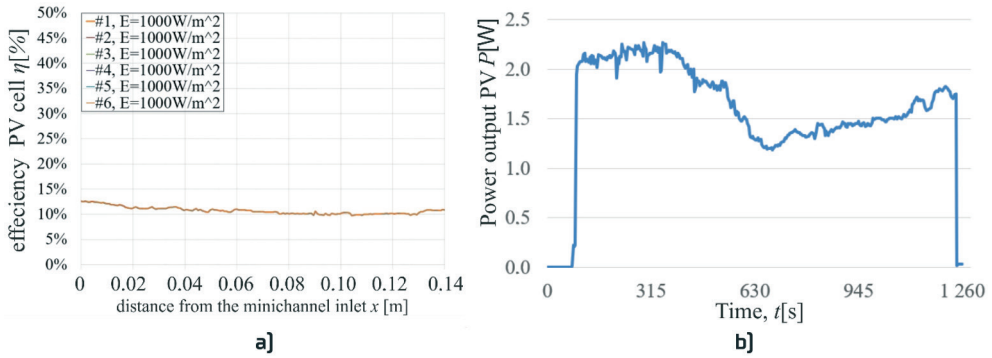

Fig 12. Diagram of the: (a) Efficiency of a cooled PV cell using a dual cooled parallel mini-channel interface, (b) power output in a non-cooled PV cell

Figure 12 shows the relationship between the heat-transfer coefficient and the efficiency of a PV cell. The heat-transfer coefficient determines how effectively the PV cell can use heat to generate electrical energy. The higher the coefficient, the better the PV cell can use heat to produce energy. On the other hand, the efficiency of a PV cell depends on many factors, such as ambient temperature, solar irradiance, PV panel quality, and the overall efficiency of the system. Generally most PV panels have an efficiency range of 15–20%, but some models can have efficiencies even above 20%. During the investigation of a cooled cell with mini-channels (as shown in Figures 8 and 9 an efficiency range of 10% to 15% was obtained for a hot fluid flow rate of m_{FC} = 0.003 kg/s and a cold fluid flow rate of m_w = 0.008 kg/s, as well as a heat flux of q = 1000 W/m^2. Figure 8b shows the ratio of the power output of a PV panel to the heating time without cooling. A power drop is visible starting at 315 seconds of heating where the power output decreased from 2.25 W to 1.22 W at 630 seconds. The heat-transfer coefficient and the efficiency of a PV cell are related because both factors affect the efficiency of converting solar energy into electrical energy. The heat-transfer coefficient at the interface between the PV cell and the fluid depends on several factors such as the FC-72 fluid, its flow rate which is m_{FC} = 0.003 kg/s, m_w = 0.008 kg/s, temperature, pressure, and the geometry of the mini-channels provided in Table 3.

5. Conclusions

To determine the values of the heat-transfer coefficient, the temperature of the fluid in the mini-channels was analyzed using Simcenter STAR-CCM+ software, which was used to carry out CFD simulations. The physical model of the heat exchanger was first pretested to ensure that the CAD model accurately represented the real system, which was then scaled to the same size. The main parameters considered in the subsequent computational analysis were meshes, physics, and geometry. These parameters were systematically varied to explore their influence on the heat-transfer efficiency of the mini-channel heat exchanger. Based on the results of the experiments and their analysis, valuable insights into the design and

https://doi.org/10.14669/AM/166810

optimization of heat exchangers with mini-channels, which are increasingly being used in various industrial applications, were obtained. The following conclusions can be drawn from this study:

- In the hot mini-channel the heat-transfer was transferred by single-phase convection and heating up the liquid occurs near the channel outlet; the heat-transfer coefficients determined for all four contact surfaces, that is, the photovoltaic cell plate – the fluid FC-72 (α_1) and the copper plate – FC-72 (α_2), copper plate-water (α_3) and the water closing plate (α_4) increased with increasing heat flux regardless of the calculation method chosen.

- In the cold mini-channel the temperature differences between plates and distilled water were low, as single-phase convection occurs in the entire mini-channel.

- The resulting heat-transfer coefficient at the heated plate – fluid FC-72 interface α_1 reached values on the order of 200 W/(m^{2}K) to a minimum of more than 7.6 W/(m^{2}K).

- In preliminary research it is assumed that the AGM battery is in good condition and its capacity is 120 Ah. The ambient temperature during the measurement was 22°C, and with a charging voltage of 13.88 V and a charging current of 15 A, the charging power will be approximately 208 W. With this charging, it can be expected that the battery temperature will increase to about 34°C without refrigeration. The temperatures at the input and output of the battery heat exchanger, used for heating the battery during the measurement, were 22.5°C and 24.2°C, respectively. For the cooling variant of the exchanger with the battery, the input temperature was 18.7°C and the output temperature 20.2°C was optimal to batteries.

- Compared with the corresponding coefficients from the 1D approach, the numerical Simcenter STAR CMM+ approach shows higher heat-transfer coefficients in both mathematical approaches, and the calculation results are similar.

- For the heat-transfer coefficients on the heated plate – FC-72 contact surface (α_1), the maximum relative differences between the results do not exceed 77.1%. In the comparative analysis of the 1D approach and numerical simulation, the lowest score percentage of 7.6% was obtained for the #3 and #4 photovoltaic center cell surface, where all heat-transfer coefficients were at their minimum.

The efficiency range of the cooled solar cell obtained was from 10% to 14%, and compared to the research of other authors, this result is better. The operating temperature range of 19.6 to 22.4 degrees Celsius is quite favorable for photovoltaic panel operation with approximate solar irradiance parameters for the latitude of Poland. Low-boiling FC-72 fluid was used in the cooling mini-channels, and water was used in the cold inlet mini-channels. A more efficient Copper (Cu) center plate material was also utilized. Additionally, the cooling employed may contribute to reducing heat losses and increasing efficiency.

https://doi.org/10.14669/AM/166810

- For a solar cell with cooling, the temperature range is from 19.6°C to 25.4°C. In this case, the temperature coefficient of efficiency is relatively low, at around –0.2%/°C, meaning that as temperature increases by 1°C, the power output of the solar cell decreases by 0.2%. For a solar cell without cooling, the temperature range is from 36.5°C to 54.8°C. In this case, the temperature coefficient of efficiency is significantly higher, at around –0.5%/°C, meaning that as temperature increases by 1°C, the power output of the solar cell decreases by 0.5%.

- Therefore, the research and methods presented in the article on mini–channel cooling of photovoltaic systems and autonomous vehicle systems are innovative at a global scale, and are crucial for further development of sustainable energy systems and reduction of greenhouse gas emissions.

In the context of heat–transfer studies, the test module can also be employed to assess the effectiveness of enhanced plate surfaces and different materials in heat exchanger applications. The test module provides a valuable tool for accelerating research and development efforts in both the automotive and heat–transfer industries. Further studies will also include modification of the mathematical model and enhanced battery heat exchange. The hybrid PVT heat exchanger is a promising solution for autonomous vehicles. By integrating photovoltaic panels and thermal collectors, this system can produce both electrical and thermal energy simultaneously, allowing for the powering of the vehicle and providing a comfortable cabin temperature. Research findings suggest that the hybrid PVT heat exchanger can be an effective way to increase the range and energy independence of autonomous vehicles. However, there are technical and economic challenges that need to be addressed for this system to be widely adopted in practice. Research on solar cell efficiency, which has been presented, may be important for the autonomous vehicle sector for several reasons. Firstly, solar cells can be used in autonomous vehicles to charge batteries, which would increase their range and enable longer journeys without the need for charging. Secondly, in the case of autonomous vehicles that operate without a driver, achieving maximum efficiency is important to minimize the impact on the payload and ensure reliable and stable real–time power supply. Additionally, in the case of autonomous vehicles that operate in challenging conditions such as very high or very low temperatures, solar cell efficiency can play a crucial role in maintaining proper power supply to the vehicle systems. The presented research can also help increase sustainable electricity production and contribute to environmental protection. Further research will focus on cooling the energy storage system of autonomous vehicles and modernizing the cooling system of photovoltaic cells to adapt them for autonomous vehicles.

https://doi.org/10.14669/AM/166810

6. Nomenclature

A surface area, m^2
E radiation intensity, W/m^2
I current, A
k overall heat-transfer coefficient, W/(m^{2}K)
L length of the mini-channel, m
p pressure, Pa
P power, W
m mass flow rate, kg/s
q heat flux, W/m^2
T temperature, K
ΔU voltage drop, V
x coordinate in the direction of flow, m

Greek letters

α heat-transfer coefficient, W/(m^{2}K)
Δ difference
δ thickness, depth, m
η efficiency of the solar cell, %
λ thermal conductivity, W/(mK)
μ dynamic viscosity, Pa·s
ρ density, kg/m3

Subscripts

a ambient
Cu copper plate
FC FC-72 fluid
H heated plate
g glass
in at the inlet
IR thermal-imaging camera
l liquid
lin *l*inear function
out at the outlet
Si silicon
STAR numerical Simcenter STAR CCM+
TC Thermocouple
v vapour
w water
1 contact surface: photovoltaic panel plate (heated plate) – FC-72
2 contact surface: FC-72 – copper center plate
3 contact surface: copper center plate – water
4 contact surface: water – closing plate (cooper plate)
1D one-dimensional approach

https://doi.org/10.14669/AM/166810

7. References

[1] Akbarzadeh A., Wadowski T.: Heat pipe-based cooling systems for photovoltaic cells under concentrated solar radiation. Applied Thermal Engineering. 1996, 16(1), 81–87, DOI: 10.1016/1359-4311(95)00012-3.

[2] Bai Y., Chow T., Menezo C., Dupeyrat P.: Analysis of a Hybrid PV/Thermal Solar-Assisted Heat Pump System for Sports Center Water Heating Application. Hindawi Publishing Corporation, International Journal of Photoenergy. 2012, 2012, 265838, DOI: 10.1155/2012/265838.

[3] Bergene T., Løvvik O.M.: Model calculations on a flat-plate solar heat collector with integrated solar cells. Solar Energy. 1995, 55(6), 453–462, DOI: 10.1016/0038-092X(95)00072-Y.

[4] Bielski J.: Wprowadzenie do inżynierskich zastosowań metody elementów skończonych. (Introduction to engineering applications of the finite element method). Politechnika Krakowska im. Tadeusza Kościuszki, Kraków. 2010, 122.

[5] Bigorajski J., Chwieduk, D.: Analysis of a micro photovoltaic/thermal – PV/T system operation in moderate climate, Renewable Energy. 2019, 137, 127–136, DOI: 10.1016/j.renene.2018.01.116.

[6] Chow T.T.: A review on photovoltaic/thermal hybrid solar technology. Applied Energy. 2010, 87(2), 365–379, DOI: 10.1016/j.apenergy.2009.06.037.

[7] Chow T.T., Tiwari G.N., Menezo C.: Hybrid Solar: A review on photovoltaic and thermal power integration. International Journal of Photoenergy. 2012, 2012, 307287, DOI: 10.1155/2012/307287.

[8] Dang T., Teng J.T.: The effects of configurations on the performance of microchannel counter-flow heat exchangers-An experimental study. Applied Thermal Engineering. 2011, 31(17–18), 3946–3955, DOI: 10.1016/j.applthermaleng.2011.07.045.

[9] Demirdzic I., Ivankovic A., O'Dowd N.: Lecture notes for the course Computational Continuum Mechanics (CCM) UCD School of Electrical. Irlandia: University College w Dublinie. Available at: https://www.scribd.com/document/442723685/CCM-I-Lecture-Notes-pdf, (access on 30.04.2023).

[10] Duan J., Zhao J., Li X., Panchal S., Fowler M., Yuan X., et al.: Modeling and Analysis of heat dissipation for liquid cooling lithium-Ion batteries. Energies. 2021, 14(14), 4187, DOI: 10.3390/EN14144187.

[11] Garg H.P., Adhikari R.S.: Conventional hybrid photovoltaic/thermal (PV/T) air heating collectors: Steady-state simulation. Renewable Energy. 1997, 11(3), 363–385, DOI: 10.1016/S0960-1481(97)00007-4.

[12] Garg H.P., Adhikari R.S.: Performance analysis of a hybrid photovoltaic/thermal (PV/T) collector with integrated CPC troughs. International Journal of Energy Research. 1999, 23(15), 1295–1304, DOI: 10.1002/(SICI)1099-114X(199912)23:15<1295::AID-ER553>3.0.CO;2-T.

[13] Hassan A., Wahab A., Qasim A.M., Janjua M.M., Ali A.M., Ali H.M., et al.: Thermal management and uniform temperature regulation of photovoltaic modules using hybrid phase change materials-nanofluids system. Renewable Energy. 2020 145, 282–293, DOI: 10.1016/j.renene.2019.05.130.

[14] Hauser J.: Podstawy elektrotermii i techniki świetlnej. (Basics of Electrothermal and Lighting Techniques). Wydawnictwo Politechnika Poznańska. Poznań, 2006.

[15] Herez A., Hage H.E., Lemenand T., Ramadan M., Khaled M.: Review on photovoltaic/thermal hybrid solar collectors: Classifications, applications and new systems. Solar Energy. 2020, 207, 1321–1347, DOI: 10.1016/j.solener.2020.07.062.

[16] Hollick J.C.: Solar cogeneration panels. Renewable energy. 1998, 15(1–4 pt 1), 195–200, DOI: 10.1016/S0960-1481(98)00154-2.

[17] Li Q., Avramova M., Jiao Y., Chen P., Yu J., Pu Z., et al.: CFD prediction of critical heat flux in vertical heated tubes with uniform and non-uniform heat flux. Nuclear Engineering and Design. 2018, 326, 403–412, DOI: 10.1016/j.nucengdes.2017.11.009.

[18] Li Y., Zhou Z.,Wu W.T.: Three-dimensional thermal modeling of Li-ion battery cell and 50 V Li-ion battery pack cooled by mini-channel cold plat. Applied Thermal Engineering. 2019, 147, 829–840, DOI: 10.1016/j.applthermaleng.2018.11.009.

[19] Madejski P.: Wymiana ciepła. (Heat exchange). Państwowe Wydawnictwo Naukowe. Warszawa-Poznań, 1975.

[20] Merkisz J., Bajerlein M., Daszkiewicz P.: The Influence of the Application of Photovoltaic Cells in City Buses to Reduce Fuel Consumption – (CO2) and Exhaust Emissions (HC, PM, and NOx). International Conference on Power and Energy Systems, Lecture Notes in Information Technology. 2012, 13, 106–113.

[21] Mikielewicz D., Wais J.: Wybrane zagadnienia projektowania mikrostrugowych wymienników ciepła. (Selected issues of designing micro-jet heat exchangers). Instytut Maszyn Przepływowych PAN w Gdańsku. Gdańsk, 2015.

[22] Pang W., Yu H., Zhang Y., Yan H.: Solar photovoltaic based air cooling system for vehicles, Renewable Energy. 2019, 130, 25–31, DOI: 10.1016/j.renene.2018.06.048.

[23] Piasecka M., Hożejowska S., Pawińska A., Strąk D.: Heat transfer analysis of a co-current heat exchanger with two rectangular mini-channels. Energies. 2022, 1340, 15(4), 1–18, DOI: 10.3390/en15041340.

[24] Piasecka M., Strąk K.: Characteristics of refrigerant boiling heat transfer in rectangular mini-channels during various flow orientations. Energies. 2021, 14(16), 4891, DOI: 10.3390/en14164891.

[25] Prakash J.: Transient analysis of a photovoltaic-thermal solar collector for co-generation of electricity and hot air/water. Energy Conversion and Management. 1994, 35(11), 967–972, DOI: 10.1016/0196-8904(94)90027-2.

[26] Prasetyo S.D., Prabowo A.R., Arifin Z.: The use of a hybrid photovoltaic/thermal (PV/T) collector system as a sustainable energy-harvest instrument in urban technology. Heliyon. 2023, 9(2), e13390, DOI: 10.1016/j.heliyon.2023.e13390.

[27] Radziemska E.: Performance Analysis of a Photovoltaic-Thermal Integrated System. International Journal of Photoenergy. 2009, 732093, DOI:10.1155/2009/732093

[28] Ratajczak J., Domke K.: Model cieplny ogniw PV i kolektorów. (The thermal model of PV cells and collectors). Electrical Engineering. 2012, 1(70), 291–298.

[29] Rockendorf G., Sillmann R., Podlowski L., Litzenburger B.: PV-hybrid and thermoelectric collectors. Solar Energy. 1999, 67(4–6), 227–237, DOI: 10.1016/s0038-092x(00)00075-x.

[30] Skoplaki E., Palyvos J.A.: On the temperature dependence of photovoltaic module electrical performance: A review of efficiency/power correlations. Solar Energy. 2009, 83(5), 614–624, DOI: 10.1016/j.solener.2008.10.008.

[31] Skoplaki E., Palyvos J.A.: Operating temperature of photovoltaic modules: A survey of pertinent correlations. Renewable Energy. 2009, 34(1), 23–29. DOI: 10.1016/j.renene.2008.04.009.

[32] Strąk D., Hożejowska S., Pawińska A.: Badania przepływowego wymiennika ciepła z minikanałami. (Research of a flow heat exchanger with mini-channels). Monografia konferencyjna XVI Sympozjum Wymiany Ciepła i Masy: Postępy w badaniach wymiany ciepła i masy. Politechnika Białostocka, Białystok, 2022, 276–286, DOI: 10.24427/978-83-67185-30-1_29.

[33] Strąk K., Piasecka M.: Boiling heat transfer during flow of distilled water in an asymmetrically heated rectangular minichannel. EPJ Web of Conferences. 2017, 143, 02116, DOI: 10.1051/epjconf/201714302116.

[34] Suman S., Goel A., Kushwah Y.S.: Design Optimization of Battery Thermal Management System for Electric Vehicles. SAE Technical Papers. 2021, DOI: 10.4271/2021-28-0123.

[35] Tarabsheh A., Etier I., Fath H., Ghazal A., Morci Y., Asad M., et al.: Performance of photovoltaic cells in photovoltaic thermal (PVT) modules. IET Renewable Power Generation. 2016, 10(7), 1017–1023, DOI: 10.1049/iet-rpg.2016.0001.

https://doi.org/10.14669/AM/166810

[36] Waseem M., Sherwani A.F., Suhaib M.: Integration of solar energy in electrical, hybrid, autonomous vehicles: a technological review. SN Applied Sciences. 2019, 1(11), 1459, DOI: 10.1007/s42452-019-1458-4.

[37] Widyolar B., Jiang L., Brinkley J., Hota S.K., Ferry J., Diaz G., et al.: Experimental performance of an ultra-low-cost solar photovoltaic-thermal (PVT) collector using aluminum minichannels and nonimaging optics. Applied Energy. 2020, 268, 114894, DOI: 10.1016/j.apenergy.2020.114894.

[38] Wiśniewski S., Wiśniewski T.S.: Wymiana ciepła. (Heat exchange). Wydawnictwa Naukowo-Techniczne. Warszawa, 2012.